Chemical Engineering Journal 160 (2010) 834–844

Contents lists available at ScienceDirect

Chemical Engineering Journal

journal homepage: www.elsevier.com/locate/cej

Residence time distributions in microchannels: Comparison between channels with herringbone structures and a rectangular channel

Alberto Cantu-Perez, Simon Barrass, Asterios Gavriilidis*

Department of Chemical Engineering, University College London, Torrington Place, WC1E 7JE, United Kingdom

ARTICLE INFO

Article history:
Received 8 December 2008
Received in revised form 26 June 2009
Accepted 9 July 2009

Keywords:
Residence time distribution
Microchannel
Herringbones

ABSTRACT

Residence time distributions (RTD) have been determined numerically and experimentally for channels with and without herringbone structures. Computational fluid dynamics (CFD) and particle tracking with random walk diffusion were employed for the numerical calculation of the RTD. The axial dispersion exchanging mass with a stagnant zone model was shown to fit the particle tracking data for the channels with staggered herringbone structures. This model provides a simpler method for RTD characterisation. Experimental RTD measurements were performed by monitoring the concentration of a tracer dye by means of a LED-photodiode system. For all cases, the calculations agreed well with experiments. The results show that for low Peclet numbers ($Pe < 10^2$) the use of herringbone structures does not have an impact on the RTD, however at high Peclet numbers ($Pe > 10^2$), channels with herringbone structures exhibit a narrower RTD than a plain channel of the same dimensions. Thus, at high Pe, inclusion of herringbones to the bottom floor of rectangular channels allows the increase in channel dimensions without adverse effect on the RTD behaviour or reaction performance.

1. Introduction

Over the last few years miniaturisation of chemical processes has been the subject of intensive research. Due to the small dimensions of the channels, the surface to volume ratio is several orders of magnitude greater than in conventional equipment leading to enhanced heat and mass transfer and higher reaction yields [1]. Residence time distributions (RTD) have been largely utilised to characterise the flow behaviour in reactors since the pioneering work by Danckwerts [2]. Since reaction conversion and selectivity are strongly affected by the RTD it is important to have an accurate description of it. The axial dispersion model proposed by Taylor [3] and modified by Aris [4] has been extensively used for description of RTD in tubular reactors that deviate from plug flow behaviour. Levenspiel and Smith [5] provided the analytical solution to the RTD of long circular channels subject to axial dispersion. Modifications to the axial dispersion model have been suggested recently to adapt it to geometries typical of microchannels [6].

Microchannels usually exhibit laminar flow. At this regime, mixing occurs only by molecular diffusion and the RTD can be broad at very low and very high radial Peclet numbers [7]. Residence time distributions in microchannels with Taylor (segmented gas–liquid) flow have been studied by various investigators both theoretically and experimentally [8–11]. Due to the recirculation patterns generated in the liquid slugs the microchannels act as series of batch reactors where a small amount of dispersion is present due to the communication of adjacent slugs with a thin liquid film. Salman et al. [10] studied the effect of different parameters on the RTD of a Taylor flow microreactor. It was found that increasing the Peclet number ($Pe = u_b d/D$) the Capillary number ($Ca = \mu u_b/\gamma$) or the slug length increased the spread of the RTD. Traschel et al. [9] measured the RTD experimentally for gas–liquid flow and compared it with the case of single phase flow, demonstrating that the variance of the RTD for gas–liquid flow was lower than for the single phase case.

For single phase flow Adeosun and Lawal [12] showed theoretically that microstructured packed bed configurations exhibit a narrower RTD as compared to a simple microchannel. Boškovic and Loebbecke [13] investigated the RTD of three different split-and-recombine micromixers by fitting an empirical model to experimental data. It was found that for all cases the RTD became narrower by increasing the flow rate due to the formation of secondary flows causing chaotic advection. Stroock et al. [14] proposed a chaotic mixer which consisted of staggered herringbone structures patterned on the floor of the microchannel. It was shown that this staggered herringbone mixer minimised dispersion at high Peclet numbers compared to a rectangular microchannel.

Several articles have characterised the mixing behaviour of the staggered herringbone mixer [15–26]. However, only few studies

* Corresponding author. Tel.: +44 0 20 7679 3811; fax: +44 0 20 7383 2348.
E-mail address: a.gavriilidis@ucl.ac.uk (A. Gavriilidis).

1385-8947/$ – see front matter © 2009 Elsevier B.V. All rights reserved.
doi:10.1016/j.cej.2009.07.023

Nomenclature

C	concentration (arbitrary units)
C_{calc}	concentration obtained from model (arbitrary units)
C_{in}	concentration at the inlet (arbitrary units)
C_{out}	concentration at the outlet (arbitrary units)
C^*	concentration in stagnant zone (arbitrary units)
$\hat{C}$	normalised concentration (1/s)
D	diffusion coefficient (m^2/s)
D_{ax}	axial dispersion coefficient (m^2/s)
d	characteristic dimension (width for rectangular channels) and diameter for cylindrical) (m)
E	age distribution function (1/s)
E_{tw}	age distribution function measured through the wall (1/s)
f	fraction of volume subject to plug flow (–)
$\mathcal{F}$	Fourier transform
F	transfer function (–)
g	scalar value dependent of the aspect ratio of geometry (–)
h	channel height (m)
I	intensity of light measured by the detector (–)
K	mass transfer coefficient between the flowing volume and the stagnant zone (s^{-1})
k	reaction rate (s^{-1})
L	length (m)
n	total number of time intervals (–)
N	total number of particles (–)
t	time (s)
t'	time spent inside the region of interest for calculation of $E(t)$ from deconvolution (s)
t_m	mean residence time (s)
t'_m	hydraulic residence time (V/v_0) (s)
T	half of the time at which the tail of the distribution vanishes (s)
U_m	mean axial velocity (m/s)
u_b	bubble velocity (m/s)
v	velocity of particles (m/s)
v_0	volumetric flowrate (m^3/s)
V	volume (m^3)
w	channel width (m)
$\vec{x}$	vector of particle position (m)
$\bar{x}$	mean conversion for a first order chemical reaction (–)
y	axial coordinate (m)

Greek letters

γ	surface tension (N/m)
μ	viscosity (Pa·s)
ρ	density (kg/m^3)
σ^2	variance (s^2)
σ^2_θ	dimensionless variance (–)
θ	dimensionless time (t/t_m) (–)
ξ	random number (zero mean and unit variance) (–)
Δt_i	time interval $t_{i+1}-t_i$ (s)

Dimensionless numbers

G	$= \frac{KL}{U_m}$
Pe	$= \frac{U_m d}{D}$
Pe_L	$= \frac{U_m L}{D_{ax}}$
Re	$= \frac{U_m d \rho}{\mu}$
β	$= Pe_L^2 + 4s\phi Pe_L t_m$
ϕ	$= f + \frac{G(1-f)}{t_m s(1-f)+G}$

characterise its residence time distribution and its possible use to minimise dispersion. Stroock and McGraw [27] presented an approximate analytical model, called "lid-driven cavity model", that mimics the effect of the grooves on the flow behaviour. They found that the patterned geometry (the microchannel floor with the grooves) can be replaced by a flat wall with an effective slip boundary condition representing the movement of the fluid caused by the grooves. The convection of massless particle tracers was used to characterise the flow behaviour. A comparison of the distribution of tracers at several cross-sections along the microchannel with experimental results showed that the model represented well the mixing characteristics of the staggered herringbone microchannel. They also presented RTD results for the staggered herringbone microchannel with different degrees of asymmetry and compared them to that of a rectangular microchannel. It was shown that all the channels with herringbone structures had a narrower RTD than the rectangular microchannel. Aubin et al. [20] using particle tracking confirmed that the RTD of the staggered herringbone microchannel approaches that of plug flow. They further observed that neither the groove depth nor the number of grooves per cycle affected the RTD significantly, in contrast with the groove width. These analyses are valid in the limit of $Pe \sim \infty$ since particle tracking considers only the movement of the particles by convection. However, as the characteristic dimension of the microchannel decreases so does Pe and the assumption that convection dominates over diffusion is no longer valid. In this case, for mixing applications diffusion would be beneficial, while from the RTD point of view diffusion may be detrimental. The RTD is not properly accounted with a pure particle tracking method because the volume of the grooves may appear to be dead space, while in reality, material will seep out from the grooves by diffusion creating a long tail in the RTD.

Residence time distributions are usually obtained by injecting an inert tracer at the channel inlet and measuring its concentration at the outlet. Different approaches for the tracer introduction and the recording of the outlet concentration have been presented for microchannels. Günther et al. [28] used a T-junction along with computer controlled syringe pump switching for the introduction of the tracer and an LED-photodiode system for the measurement of tracer concentration. Trachsel et al. [9] injected the tracer as a Dirac-delta pulse by a piezoelectrically actuated membrane and recorded its concentration by fluorescence microscopy. Boškovic, and Loebbecke [13] injected the tracer with an HPLC valve and recorded its concentration by an in-house made UV–vis flow-through cell. Lohse et al. [29] described a novel method for the determination of the RTD based on the optical activation of a caged fluorescence dye. Tracer concentration was determined by fluorescence microscopy. This method allows for the determination of RTD without the need of measuring the inlet signal because the inlet is ensured to be a Dirac-delta pulse.

In this work, the RTD of a rectangular channel is compared with that of channels with floor herringbone structures (see Fig. 1). Residence time distributions are obtained experimentally by means of a LED-photodiode array system and numerically by CFD simulations with particle tracking. The effect of geometrical parameters, herringbone symmetry and operational parameters on the RTD is investigated.

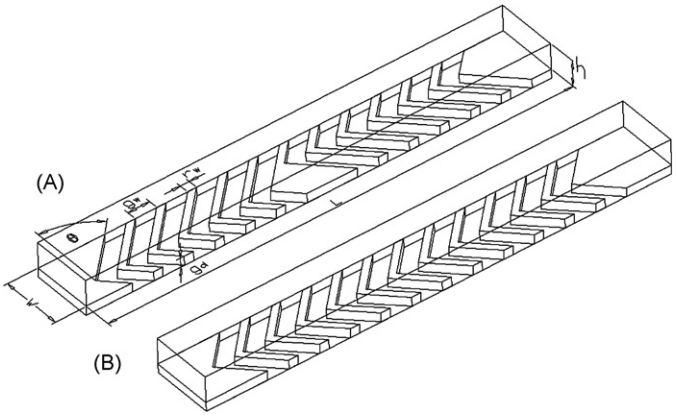

Fig. 1. (A) Geometry of the staggered herringbone channel. (B) Geometry of the symmetric herringbone channel. Fluid travels from left to right.

2. Theoretical approach

Two different theoretical approaches were employed for the calculation of the RTD. The first one is completely numerical, relying on the solution of the Navier–Stokes equations and a particle tracking algorithm. The second one is based on a hydrodynamic model with adjustable parameters which are fitted using experimental or particle tracking data.

2.1. Numerical particle tracking method

The channel with the staggered herringbone structure (Fig. 1A) is similar to the one proposed by Stroock et al. [14]. The channel is divided in cycles, each one consisting of twelve asymmetric grooves. The position of the asymmetry changes every half cycle. In Fig. 1B a schematic of a symmetric herringbone structure is presented. The grooves in both structures are placed at an angle $\theta = 45^\circ$ with respect to the channel width. The groove depth is 0.17 mm, the groove width is 0.7 mm and the ridge width is 0.3 mm (measured along the axial direction). In addition to the herringbone floor channels, an unstructured rectangular channel is also considered. The widths of the channels are 2 mm for all cases and their heights are 0.84, 0.71 and 0.81 mm for the rectangular, symmetrical and staggered herringbone channels respectively. All the above dimensions correspond to experimentally determined values of microchannels used in the experiments and are summarised in Table 1. Due to the repeating cycles, the velocity field is assumed to be periodic and hence the velocity field in one cycle can be obtained and used repeatedly for successive cycles. The fluid properties of water were used for all simulations with density $\rho = 1000\ \mathrm{kg/m^3}$ and viscosity $\mu = 0.001$ Pa·s.

The residence time distribution $E(t)$, can be calculated by solving the velocity field for the particular geometry and tracking the positions of massless particles convected by the flow. It has been shown by Levenspiel and Turner [30] that to obtain the correct RTD when the velocity profile after the injection and measurement point is not flat (for example in laminar flow) the number of particles introduced must be proportional to the velocity at each radial injection position and the measurement must be the mixing cup reading. For this reason 4400 particles are distributed proportionally to the axial velocity at the channel inlet. The locations of the particles are computed by integrating the equation of motion:

$$\frac{d\vec{x}}{dt} = v(\vec{x}) \tag{1}$$

The Navier–Stokes and the continuity equation for the conservation of mass, are solved simultaneously with COMSOL Multiphysics 3.3 for a full cycle (see Fig. 1). No-slip boundary conditions are applied to all walls and periodic boundary conditions were considered at the inlet and outlet. This allows using the simulated velocity field for one cycle, over many successive cycles if entrance effects are neglected. The volumetric flowrate is calculated by integrating the velocity profile which is obtained after specifying a pressure drop across the cycle and setting the outlet pressure equal to the inlet pressure minus the specified pressure drop. 34,582 of tetrahedral mesh elements were used in the model and the simulations were run on Windows XP with Pentium IV 3.00 GHz CPU and 2 GB of RAM. At this number of elements the solution was found to be mesh independent**.** The solution is exported to MATLAB where a particle tracking algorithm obtains the velocity at the position of the particle by interpolation and gets its new position by solving Eq. (1) for a fixed time step. A time step corresponding to an average distance travelled $\overline{\Delta x} = 0.17h$ was found to be sufficient, as smaller time steps did not change the RTD results. The positions of the particles and their time of arrival at a particular location are recorded and the procedure is repeated over a specified number of steps. This code is set so that the velocity field obtained for the first cycle could be used over many cycles. A standard fourth order Runge–Kutta method with fixed time steps was used to get the solution of (1).

The particle tracking algorithm described by Eq. (1) may be modified so that the particles have a convective transport and a random diffusion step. This approach has been used to approximate diffusion [31,32]. Therefore Eq. (1) is modified and the particle trajectories are calculated with the following stochastic differential equation [33]:

$$d\vec{x} = v\left(\vec{x}\right) dt + \sqrt{2Ddt}\xi \tag{2}$$

where D is the diffusion coefficient and ξ is a random number with zero mean and unit variance. If a particle leaves one of the boundaries of the channel, it is reflected back to its previous position. In this way the total number of particles is conserved. Eq. (2) approxi-

Table 1
Dimensions of microchannel geometries studied and fluid properties.

	Rectangular channel	Staggered heringbone channel	Symmetrical herringbone channel
Channel width, w	2 mm	2 mm	2 mm
Channel height, h	0.84 mm (±) 2%	0.81 mm (±) 7%	0.71 mm (±) 7%
Length per cycle	1.516 mm	1.516 mm	1.516 mm
Number of grooves per cycle	–	12	12
Groove width, g_w	–	0.7 mm (±) 2%	0.7 mm (±) 2%
Ridge width, r_w	–	0.3 mm (±) 2%	0.3 mm (±) 2%
Groove depth, g_d	–	0.17 mm (±) 25%	0.17 mm (±) 16%
Groove Asymmetry	–	2/3	2/3
Groove angle, θ	–	45°	45°
Fluid Properties			
Density	1000 kg/m^3		
Viscosity	0.001 Pa·s		

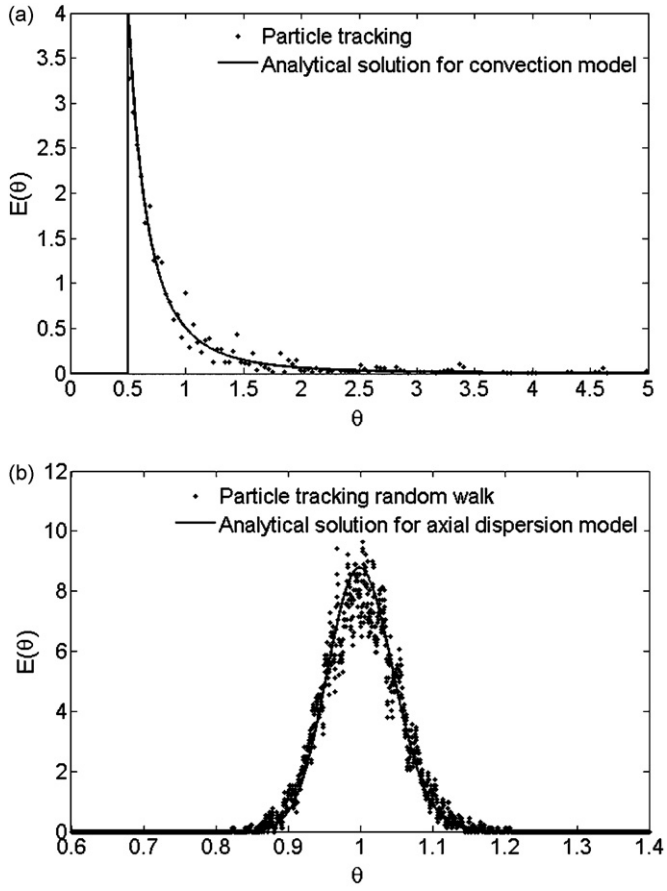

Fig. 2. Dimensionless RTD of particle tracking methods and analytical solutions for a cylindrical channel. (a) Convection model vs. particle tracking simulation. (b) Dispersion model vs. particle tracking with random walk simulation.

mates the solution to the convection–diffusion equation as the time step approaches zero. Due to the stochastic nature of the calculations an average of three runs is considered for all particle tracking simulations yielding an error on the calculated mean residence time of ±1.2%. Once the number of particles arriving at the channel exit, N_i, as a function of time interval, $\Delta t_i = t_{i+1} - t_i$, is obtained the RTD can be calculated from:

$$E(t_i) = \frac{N_i}{\sum_{i=1}^{n} N_i \Delta t_i} \tag{3}$$

where n is the total number of time intervals. The RTD in dimensionless form is obtained from:

$$E(\theta) = t_m E(t_i) \tag{4}$$

where t_m is the mean residence time.

Fig. 2 shows a comparison of both particle tracking methods (i.e. with or without random walk diffusion) with available analytical solutions for a 100 μm diameter cylindrical channel with no diffusion (convective regime) [7] and with a diffusion constant of $D = 5 \times 10^{-9}$ m^2/s for Pe = 30 [5]. Measurements are made at a dimensionless length of $L/d = 45$. The agreement of both methods with the analytical solutions is satisfactory. Particle tracking with random walk diffusion is used for all subsequent calculations, because it can incorporate the effect of mass transfer by diffusion in the RTD, while the standard particle tracking method is only valid in the limit of no diffusion or Pe ∼ ∞.

2.2. Analytical method

Analytical expressions for the RTD for ideal reactors (CSTR, convective model, plug flow) are available in the literature. A comprehensive review of the flow system models for chemical reactors is given by Wen and Fan [34]. The axial dispersion model is commonly used to describe the behaviour in tubular reactors that deviate from plug flow and is characterised by a dispersion mechanism acting on the axial direction. The governing equation of this model is:

$$\frac{\partial C}{\partial t} = D_{ax}\frac{\partial^2 C}{\partial y^2} - U_m\frac{\partial C}{\partial y} \tag{5}$$

Taylor [3] and Aris [4] provided analytical expressions for the determination of the axial dispersion coefficient in cylindrical tubes. Ananthakrishnan et al. [35] and Levenspiel [7] provide useful charts for the limits of application of each expression. The axial dispersion model is not suitable for RTDs exhibiting long tails. In this case the axial dispersion model exchanging mass with a stagnant volume (ADEM) is more appropriate [36–39]. It is expressed by the following system of differential equations:

$$D_{ax}\frac{\partial^2 C}{\partial y^2} - U_m\frac{\partial C}{\partial y} = f\frac{\partial C}{\partial t} + (1-f)\frac{\partial C^*}{\partial t} \tag{6}$$

$$(1-f)\frac{\partial C^*}{\partial t} = K(C - C^*) \tag{7}$$

where f is the fraction of the volume subject to plug flow with axial dispersion, C^* is the concentration in the stagnant zone and K is the mass transfer coefficient between the flowing volume and the stagnant zone. Estimating the model parameters by fitting the mea-

sured response signal $C_{out}(t)$ with the one calculated in the time domain $C_{calc}(t)$ is shown to give the most accurate results [40,41].

Applying the Laplace transform to Eqs. (6) and (7), the transfer function subject to open–open boundary conditions is [36]:

$$F(s) = \frac{2\beta^{1/2}\exp[1/2(\mathrm{Pe}_L - \beta^{1/2})]}{(\mathrm{Pe}_L + \beta^{1/2}) - (\mathrm{Pe}_L - \beta^{1/2})\exp(-\beta^{1/2})} \tag{8a}$$

where:

$$\beta = \mathrm{Pe}_L^2 + 4s\phi\mathrm{Pe}_L t_m \tag{8b}$$

$$\phi = f + \frac{G(1-f)}{t_m s(1-f)+G} \tag{8c}$$

$$G = \frac{KL}{U_m} \tag{8d}$$

$$\mathrm{Pe}_L = \frac{U_m L}{D_{ax}} \tag{8e}$$

By using the definition of the transfer function $F(s)=C_{calc}(s)/C_{in}(s)$ in the Fourier domain, which corresponds to the residence time distribution, $E(t)$, in the time domain, the calculated output signal in the time domain is obtained from an inverse Fourier transform:

$$C_{calc}(t) = \mathcal{F}^{-1}[\mathcal{F}(E(t)) \cdot \mathcal{F}(C_{in}(t))] \tag{9}$$

The continuous Fourier transform and its inverse are approximated by a fast Fourier transform using the Cooley–Tukey algorithm in Matlab. The model has three parameters: f, G and Pe_L which are obtained by minimising the root mean square error (RMSE) shown in Eq. (10)

$$\mathrm{RMSE} = \left[\frac{\int_0^{2T}(C_{out} - C_{calc})^2 dt}{\int_0^{2T}(C_{out})^2 dt}\right]^{1/2} \tag{10}$$

where $2T$ is the time at which the tail of the distribution vanishes. The criterion for convergence is when the root mean square error (RMSE) is less than 0.1 [42]. The optimisation was done in Matlab using the *fminunc* function which uses the BFGS method.

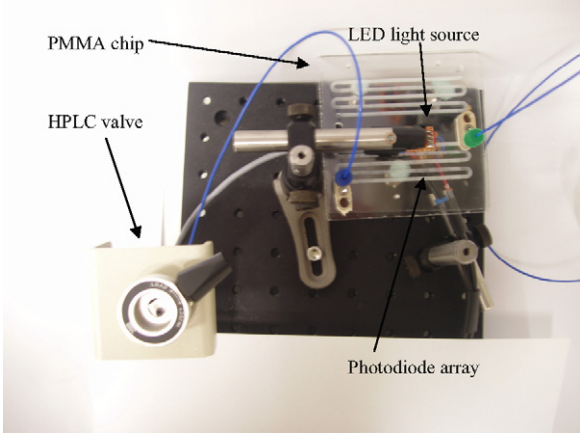

Fig. 3. Picture of the experimental set up used for RTD studies.

3. Experimental details

3.1. Set-up description

The channels were fabricated on a plate of PMMA (Polymethylmethacrylate) (RS-components), 8 cm × 8 cm × 3 mm by engraving (Roland EGX-400). The engraved PMMA plates were cleaned in an ultrasonic bath for 20 min using Decon 90 and dried with an air gun. To produce closed channels the plates were clamped, along with a top PMMA plate with feed-through holes, in a stainless steel jig and placed in an oven (Lenton WF30) for 10 min at 110 °C (close to the PMMA softening temperature) for bonding. The chips were allowed to cool slowly overnight and were ready to use the next day. The dimensions of the channels were measured with a profilometer (Veeco, Dektak 8) and are given in Table 1. An HPLC pump (Waters 510) was used for feeding deionized water to the chip (flowrates 0.5 and 1 ml/min). The tracer pulse (Parker Blue dye) was introduced by a 6-port sample injection valve (Rheodyne 7725(i)) equipped with 5 μl sample loop and an internal position signal switch that indicates the time of injection. The piping among all components was Teflon 0.254 mm ID. The hydraulic residence time in the tubing connecting the valve to the inlet of the chip was 1.5 and 7.6 s for flowrates of 0.5 and 0.1 ml/min respectively. Tracer detection was performed by light absorption. Illumination was provided by two square LEDs (Kingbright L-1553IDT). To make sure that only light going through the desired channel area was collected, black tape was used to mask the neighbouring areas. To seal the system from ambient light it was placed in a dark box. The detection system was based on a linear diode array detector (TSL, 1401R-LF) which had 128 diodes each of dimensions 63.5 μm by 55.5 μm. This was driven using the manufacturer's recommended circuit. A scan of all diodes would take 1.28 ms and the interval between successive scans was 5.12 ms. Data from the sensor was collected using a National instruments PCI-6010 data acquisition card before being analysed and displayed on a computer using a program written in Labview. Every 100 ms the computer would average the previous two scans, calculate the absorbance for each diode and display the result. The absorbance of the tracer dye was found to be in accordance with the Beer–Lambert law. A digital signal from the injection valve was also acquired to allow the absorbance data time to be referenced to the time of injection. In order to obtain the true RTD of the system, the mixing cup concentration must be measured (flux-averaged concentration). However, through the wall measurements are usually the norm in experimental set-ups such as in this work. Levenspiel et al. [43] and Levenspiel and Turner [30] have shown that, when there is a spread in longitudinal velocity (such as in laminar flow), through the wall measurements will lead to distributions skewed towards the slower moving molecules. A correction for through the wall measurements was suggested [43] that is valid when interaction between streamlines is negligible. A picture of the experimental set up is shown in Fig. 3.

The diffusion coefficient of the dye in water was obtained experimentally in a rectangular channel 21 cm × 2 mm × 0.85 mm, by first calculating the vessel dispersion number ($D_{ax}/U_m L$) by the following equation [5]:

$$\frac{D_{ax}}{U_m L} = \frac{1}{8}\left(\sqrt{8\sigma^2 + 1} - 1\right) \tag{11}$$

where σ^2 is the variance of the distribution obtained experimentally and L is the length of the region of study. The relationship between diffusivity and axial dispersion coefficient for a rectangular channel with arbitrary aspect ratio is [6]

$$D_{ax} = D + \frac{h^2 U_m^2}{210D} g \tag{12}$$

where g is a number depending on the aspect ratio of the channel and is approximately 3.8 for the conditions presented here $(h/w = 0.425)$.

3.2. Data analysis

The mean residence time can be calculated from the intensity data according to:

$$t_m = \frac{\sum_{i=1}^{n} t_i I(t_i)\Delta t_i}{\sum_{i=1}^{n} I(t_i)\Delta t_i} \quad (13)$$

where $I(t_i)$ is the intensity of light measured by the detector at each recorded time, Δt_i is defined as $t_{i+1} - t_i$ and is constant throughout the experiment. The variance may be calculated as follows:

$$\sigma^2 = \frac{\sum_{i=1}^{n} (t_i - t_m)^2 I(t_i)\Delta t}{\sum_{i=1}^{n} I(t_i)\Delta t} \quad (14)$$

which in dimensionless form is:

$$\sigma_\theta^2 = \frac{\sigma^2}{t_m^2} \quad (15)$$

The intensity measured at both the outlet and inlet is normalised to yield a normalised concentration:

$$\hat{C}(t_i) = \frac{I(t_i)}{\sum_{i=1}^{n} I(t_i)\Delta t} \quad (16)$$

The input signal to the region of interest is not a perfect Dirac-delta impulse since the injected plug is dispersed by the capillary tube from the injection point to the inlet of the channel. The output concentration is then related to the input concentration and the RTD by the convolution integral [44].

$$C_{out}(t) = \int_0^t C_{in}(t - t')E(t')dt' \quad (17)$$

The convolution integral corresponds to multiplication in the frequency domain, therefore:

$$\mathcal{F}(C_{out}(t)) = \mathcal{F}(C_{in}(t)) \cdot \mathcal{F}(E(t)) \quad (18)$$

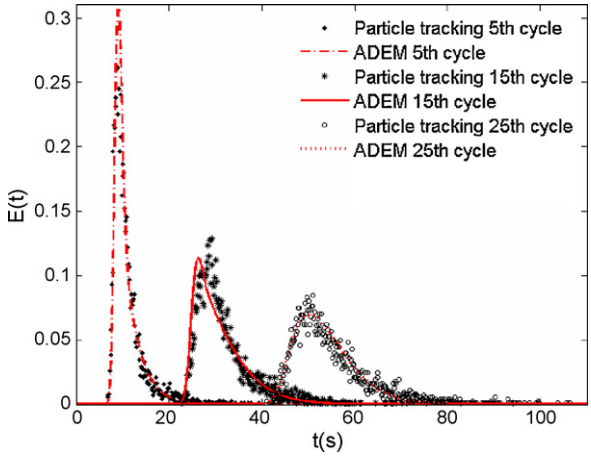

Fig. 4. Comparison of the RTD for the staggered herringbone channel obtained from the particle tracking method with random walk diffusion and the model of axial dispersion exchanging mass with a stagnant zone (ADEM) for cycles 5th, 15th and 25th (7.6, 22 and 38 cm). The parameters of the model were calculated using particle tracking results for the 15th cycle. Channel dimensions are shown in Table 1, Pe ~ 10^4.

The RTD is obtained by taking the inverse Fourier transform of Eq. (18).

$$E_{tw}(t) = \mathcal{F}^{-1}\left(\frac{\mathcal{F}(C_{out}(t))}{\mathcal{F}(C_{in}(t))}\right) \quad (19)$$

where $E_{tw}(t)$ is the age distribution curve of the region of interest obtained from experimental data measured through the wall. The Fourier transform and its inverse were approximated by a fast Fourier transform as described earlier. Deconvolution is very sensitive to noise, therefore signal filters and curve smoothing were used [45]. The parameters of the filter and the curve smoothing were chosen so that the convolution of C_{in} with $E_{tw}(t)$ resulted in C_{out}. In addition it was checked that neither the mean residence time nor the variance changed as a result of this procedure as suggested by Mills and Dudukovic [46]. The number of experimental points taken for C_{out} and C_{in} were always more than 2000 ($\Delta t = 0.1$ s) to avoid aliasing. In dimensionless form, the time and the RTD are:

$$\theta_i = \frac{t_i}{t_m} \quad (20)$$

$$E_{tw}(\theta_i) = t_m E_{tw}(t_i) \quad (21)$$

Since the RTD obtained was measured through the wall and transverse concentration profiles due to laminar flow are expected, a correction must be made in order to obtain the correct RTD. According to Levenspiel et al. [43] if both the inlet and outlet are measured through the wall the correct RTD may be obtained from:

$$E(\theta_i) = \frac{E_{tw}(\theta_i)}{\theta_i^2} \quad (22)$$

The results without this correction yield measurements which are skewed towards the right, resulting to higher average residence time and variance.

4. Results and discussion

4.1. RTD from particle tracking and hydrodynamic model

Fig. 4 shows the $E(t)$ curve obtained with the particle tracking method with random walk diffusion described in Section 2 for a channel with staggered herringbone structures (see Table 1 for dimensions) for Re = 0.013 and Pe ~ 10^4 at a distance of 7, 22 and 36 cm (5th,15th and 25th cycles) from the channel entrance. It can be seen that the particles experience a high peak followed by a long tail which is due to particles trapped in the grooves that take longer time to get out of the system. Tracking the particles for a long time might be computational expensive. For this reason, a suitable hydrodynamic model would help predict the RTD for longer times. Hence, the RTD at the 15th cycle is fitted to the ADEM model as described in Section 2.2. The values of the model parameters were calculated to be: $Pe_L = 597.7$, $G = 1.58$ and $f = 0.85$ with a mean residence time $t_m = 31.76$ s calculated with Eq. (13) replacing $I(t_i)$ with N_i. It is worth noting that the hydraulic residence time $t'_m = V/v_0$ is 37.2 s. This gives a ratio of t_m/t'_m of 0.85 which is consistent with the work of Aubin et al. [20] who found that for wide grooves (75 μm) the ratio of the calculated residence time from particle tracking to the hydraulic residence time was 0.85. Furthermore, the volume fraction of the stagnant zone in the ADEM model $(1 - f) = 0.15$ is close to the volume fraction of the channel occupied by the grooves which is 0.13. From these Pe_L and G the original model parameters (see Eqs. (6) and (7)) are found to be: $D_{ax} = 2.29 \times 10^{-8}$ m^2/s, $K = 0.052$ s^{-1}. Using these parameters, the RTD at different lengths (5th and 25th cycles) are calculated and are shown in Fig. 4. The agreement of the RTD prediction by the model at the 5th and 25th cycle is satisfactory.

In Figs. 5 and 6, RTDs obtained via particle tracking for a rectangular channel and a microchannel with staggered herringbone

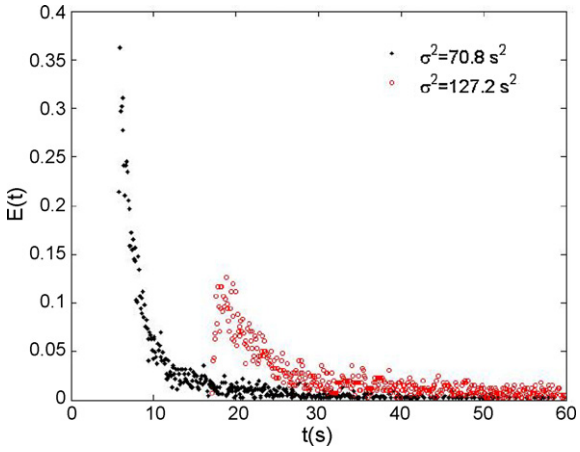

Fig. 5. Residence time distribution in the rectangular channel from particle tracking with random walk diffusion at 2 cm (●) and 6.2 cm (○). The dimensions of the channel are $w = 200\ \mu m$, $h = 85\ \mu m$. Pe $\sim 10^4$.

structures for Pe $\sim 10^4$ are shown. The microchannels are 200 μm wide and 85 μm deep for both the rectangular and the herringbone microchannels; the grooves are 50 μm wide and 31 μm deep. These dimensions are similar to those of Stroock et al. [14]. The dispersion experienced by the rectangular microchannel is higher than in the patterned microchannel as shown by the calculated variances. Note that variances are calculated by Eq. (14), where $I(t_i)$ is replaced by N_i. For the rectangular microchannel the calculated variances were 70.8 and 127.2 s^2, for 2 and 6.2 cm long microchannels respectively, while for the microchannel with staggered herringbones were 18.9 and 52.6 s^2. The RTD for the rectangular microchannel is characterised by an early peak after 6 and 18 s at 2 and 6.2 cm microchannel lengths respectively, followed by a long tail (typical of a pure convection model with no diffusion). The hydraulic residence time for these two positions is 11.27 and 33.0 s respectively. On the other hand, for the microchannel with staggered herringbones, the peaks are located at 10 and 30 s for the same microchannel positions (2 and 6.2 cm). The hydraulic residence time for these two positions is 12.2 and 35.5 s respectively. These results show that the microchannel with staggered herringbones is able to reduce dispersion; the time where the peaks are obtained are closer to the hydraulic residence time. The results are in qualitative agreement with the experimental observations of Stroock et al. [14].

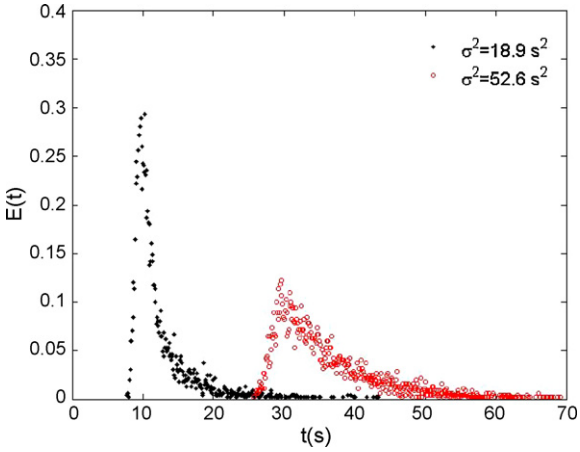

Fig. 6. Residence time distribution in the staggered herringbone channel from particle tracking with random walk diffusion at 2 cm (●) and 6.2 cm (○). The dimensions of the channel are $w = 200\ \mu m$, $h = 85\ \mu m$, $g_w = 50\ \mu m$, $g_d = 31\ \mu m$, $r_w = 50\ \mu m$. Pe $\sim 10^4$.

Table 2
Reactant conversion for a first order reaction ($k = 0.1\ s^{-1}$) in a staggered herringbone and a rectangular channel. The grooves of the staggered herringbone channel are 500 μm wide and 310 μm deep. A constant aspect ratio $h/w = 0.425$ is considered for all channels. Conversions were obtained from Eq. (23) with the RTD obtained from particle tracking at a distance of 15 cycles and a mean residence time of 12.3 s. Fluid properties were density $\rho = 1200\ kg/m^3$ viscosity $\mu = 0.067$ Pa·s.

	Conversion	Pe = $U_m d/D$	ΔP (Pa)
Plug flow	70.8%	40,000	–
Staggered herringbone channel 2 mm wide	68.8%	40,000	6,300
Rectangular 2 mm wide	64.8%	40,000	6,700
Rectangular 450 μm wide	68.6%	9,000	29,500

If we would like to have a similar RTD in the rectangular microchannel as in the staggered herringbone one, we would have to decrease the size of the unstructured channel. One way of estimating the dimensions of a rectangular microchannel that behaves similar to a microchannel with herringbone structures would be to obtain an axial dispersion coefficient from the variance of the staggered herringbone microchannel distribution as shown in Eq. (11). Then, if the diffusion coefficient is known, the characteristic dimensions of a rectangular microchannel can be obtained for any aspect ratio with Eq. (12). This analysis showed that, keeping the aspect ratio constant $(h/w = 0.425)$, the dimensions of a rectangular microchannel, that has a similar variance as a 2 mm wide staggered herringbone microchannel, would be 450 μm. One would expect that this procedure is not accurate enough since the RTD of the microchannels cannot be correctly characterised by a simple axial dispersion model. However, we found that although the shape of the RTDs for the staggered herringbone and the rectangular microchannel was different, the conversion for first order chemical reaction was the same. Since the conversion for a first order chemical reaction is uniquely determined by the reaction constant and the RTD in the reactor, it provides a basis for comparing different RTDs. The mean conversion for a first order chemical reaction of the type $A \xrightarrow{k} B$ is given by:

$$\bar{x} = 1 - \int_0^\infty e^{-kt} E(t) dt \tag{23}$$

Table 2 shows the conversions and pressure drop for a rectangular microchannel with and without herringbone structures for a reaction constant $k = 0.1\ s^{-1}$. The results show that a rectangular channel with 2 mm width has a conversion of 64.8% and a ΔP of 6700 Pa after 22 cm for Pe $\sim 10^4$ while the staggered herringbone channel achieved 68.8% with a ΔP of 6300 Pa for the same conditions. If the width of the rectangular microchannel is decreased to 450 μm, a conversion of 68.6% is achieved but with a pressure drop of $\Delta P = 29{,}500$. For comparison, a Kenics mixer with a diameter of 1.2 mm (the hydraulic diameter of the rectangular channels considered was 1.2 mm) and the same conditions considered for the rectangular channels would give a pressure drop of $\Delta P = 36{,}343$ Pa [47].

4.1.1. Effect of Pe

Although the herringbone structures prove to be an efficient way to narrow the RTD at high Peclet numbers, for smaller Peclet numbers where mass transfer by diffusion plays a more important role, channels with and without herringbones have a similar RTD as shown in Fig. 7 for Pe $\sim 10^2$ (Pe was changed by changing the diffusion constant). In this case, radial mass transfer by diffusion is substantial and there is no need to have the herringbone structures to narrow the RTD. Furthermore, for the staggered herringbone channel, at high Pe, as the Peclet number increases the RTD remains unchanged as shown in Fig. 8. This result has been pointed out recently by Vikhansky [48] who showed that for a chaotic flow the RTD is practically independent of Pe. Such behaviour opens the pos-

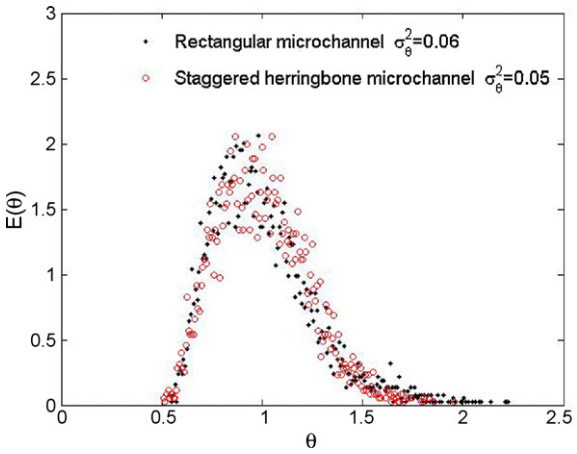

Fig. 7. Dimensionless RTD for a rectangular microchannel and the staggered herringbone microchannel from a particle tracking method with random walk diffusion. The dimensions of the channel are $w = 200$ μm, $h = 85$ μm for both channels and the groove parameters are: $g_w = 50$ μm, $g_d = 31$ μm, $r_w = 50$ μm. Pe ~ 10^2.

sibility of increasing the velocity or the hydraulic diameter of the channels (increase Pe) without compromising its performance in terms of residence time distribution.

4.1.2. Influence of geometrical parameters of grooves

A sensitivity analysis of the influence of the groove's geometrical parameters on the residence time distribution was carried out. The dimensionless variances for all cases were estimated from an average of three simulations (with an error of less than 8%) and compared to the reference case with 45° groove angle, 31 μm depth and 50 μm width at a length of 2.3 cm (15 cycles) and are shown in Table 3. At the angles of 30° and 60° the variances of the RTD are 0.0654 and 0.0194 respectively, compared to 0.0206 of the reference case**.** It seems that there is an optimum groove angle to maximise transverse fluid movement. In fact, for mixing which also is influenced by the transverse movement of fluids, a groove angle of 53° has been found to be optimal [24]. The analysis on the groove depth shows that the RTD exhibits a higher variance at low depth (15 μm) ($\sigma_\theta^2 = 0.0852$) compared to the reference case ($\sigma_\theta^2 = 0.0206$); at higher depths the variance remains nearly constant $\sigma_\theta^2 = 0.0199$ and $\sigma_\theta^2 = 0.0194$ for 43 and 60 μm depths respectively. This indicates that increasing the groove depth narrows the RTD, however there is a critical groove depth beyond

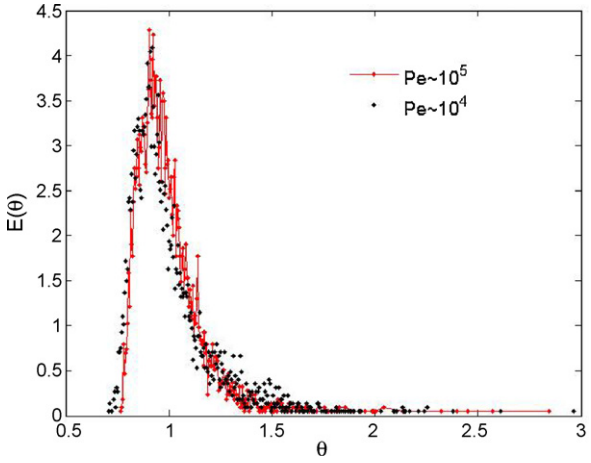

Fig. 8. Residence time distribution from particle tracking with random walk for a channel with staggered herringbone structures for Pe ~ 10^4 and Pe ~ 10^5. Channel dimensions $w = 2$ mm, $h = 0.71$ mm, groove width is 0.7 mm and depth is 0.18 mm.

Table 3
Influence of groove geometrical parameters (angle, depth and width) on the variance of the RTD. Parameters which are not specified have base case values: $\theta = 45°$, $d_g = 31$ μm, $w_g = 50$ μm, $h = 85$ μm and $w = 200$ μm. For all cases groove + ridge width was 100 μm, number of grooves = 12 and cycle length = 1.516 mm.

Influence of groove angle	$\sigma_\theta^2 = 0.0654$ $\theta = 30°$	$\sigma_\theta^2 = 0.0206$ $\theta = 45°$	$\sigma_\theta^2 = 0.0194$ $\theta = 60°$
Influence of groove depth	$\sigma_\theta^2 = 0.0852$ $g_d = 15$ μm	$\sigma_\theta^2 = 0.0206$ $g_d = 31$ μm	$\sigma_\theta^2 = 0.0194$ $g_d = 60$ μm
Influence of groove width	$\sigma_\theta^2 = 0.1113$ $g_w = 30$ μm	$\sigma_\theta^2 = 0.0206$ $g_w = 50$ μm	$\sigma_\theta^2 = 0.0517$ $g_w = 70$ μm

which the RTD is no longer improved. The results by Aubin et al. [20] also show that increasing the groove depth does not affect the RTD significantly. The groove width has a significant impact on the RTD. Both for wider and narrower grooves the distribution is worsened with respect to the reference case. Narrow grooves (15 μm wide) give the highest variance for all cases studied ($\sigma_\sigma^2 = 0.1113$) because they are unable to stir the fluid and force it to sample the whole cross-section. On the other hand, wide grooves stir the fluid efficiently as has been shown by Aubin et al. [20] and Lynn and Dandy [49]. However, although mixing is improved as the groove width is increased, the RTD is worse ($\sigma_\theta^2 = 0.0517$) with respect to the reference case, because of the increased volume of the grooves which could potentially increase dispersion by allowing a greater percentage of fluid to remain in the system for longer times. Results by Aubin et al. [20] also showed that narrow grooves have a detrimental effect on the RTD. However, they found that for wide grooves the RTD was improved. Reasons for this discrepancy maybe because in our work mass transfer by diffusion was considered and the particles are able to leave the low velocity zones by diffusion.

4.2. RTD from experiments and particle tracking model

Residence time distributions have been obtained experimentally for a rectangular channel and channels with symmetric and staggered herringbone structures at a length of 22 cm with blue dye (Parker Quink) as a tracer. Fig. 9 shows the normalised tracer inlet and outlet signal, $\hat{C}_{in}(t)$, $\hat{C}_{out}(t)$ at Pe ~ 10^4, for three separate experiments, which were very similar (measured mean residence times where within 1.1%), indicating good reproducibility. Since the injected plug is not a perfect pulse, the RTD needs to be obtained by deconvolution as discussed earlier. This procedure is accompanied by an increase in noise for this reason signal filters and curve smoothing were applied. The convolution of the RTD and the inlet

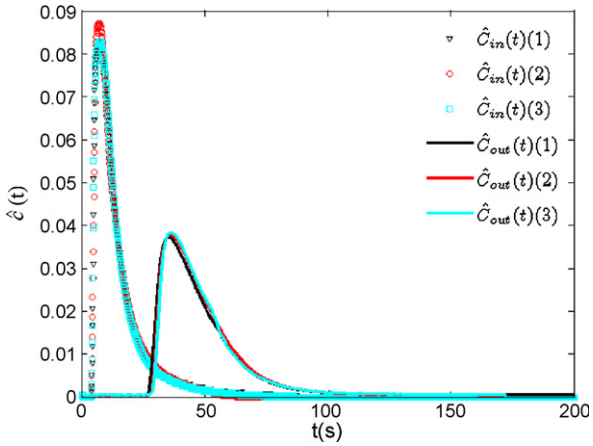

Fig. 9. Normalised tracer concentration at the inlet and outlet for the staggered herringbone channel at 22 cm for three separate experiments. Pe ~ 10^4.

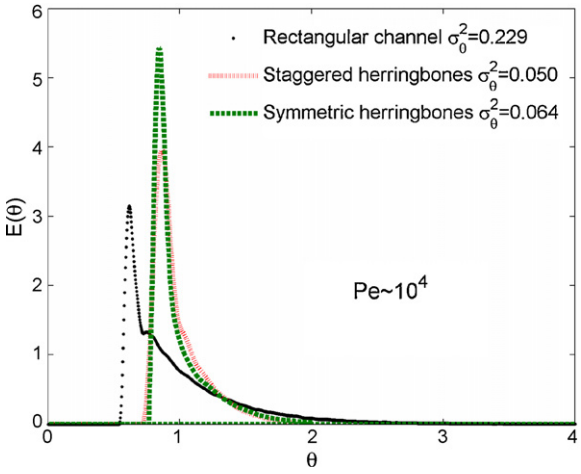

Fig. 10. Dimensionless experimental residence time distributions for a rectangular channel and channels with symmetric and staggered herringbone structures for Pe ~ 10^4. The dimensions of the channels are listed in Table 1. The distance of measurement from injection location is 22 cm.

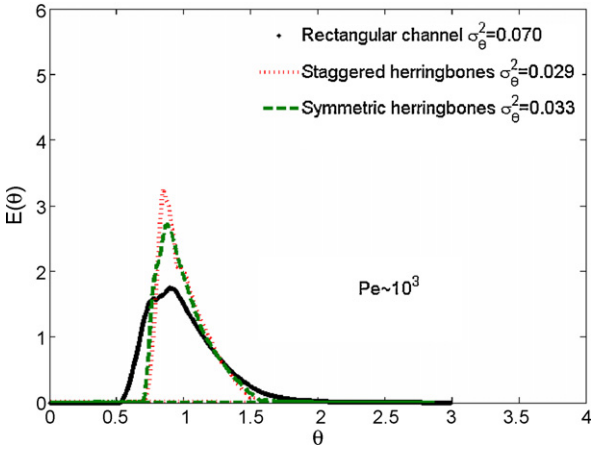

Fig. 12. Dimensionless experimental residence time distributions for a rectangular channel and a channel with symmetric and staggered herringbone structures for Pe ~ 10^3. The dimensions of the channels are listed in Table 1. The distance of measurement from injection location is 22 cm.

tracer signal reproduced exactly the outlet signal. RTDs for the three experimental devices are shown in Fig. 10. It is evident from this figure that the RTD for the rectangular channel is consistent with the asymmetry of the convective model characterised by an early peak at ca. half the mean residence time followed by a long tail. Furthermore the RTD of the channel with the staggered herringbone structures and the one with the symmetric ones is similar which is consistent with the results obtained by Stroock and McGraw [27]. The dimensionless variance, σ_θ^2, for the staggered and symmetric herringbone channels are 0.050 and 0.064 respectively much smaller than that of the rectangular channel (0.229). Although it has been shown that the symmetrical herringbone is a poor mixer [27], in terms of RTD it does a good job by achieving flow inversion through bringing material from the low to the high velocity zones and vice versa. Fig. 11 shows a comparison between the experimen-

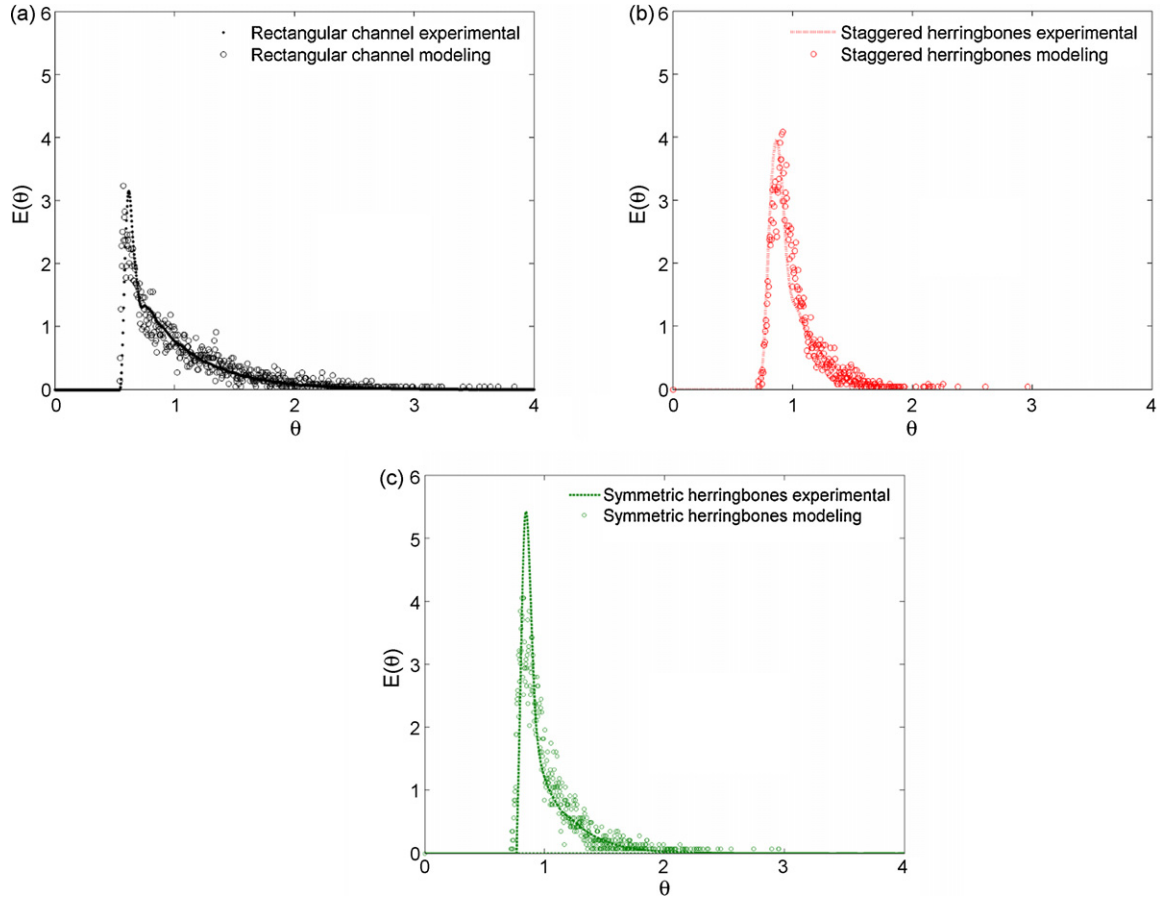

Fig. 11. Comparison of the dimensionless residence time distributions obtained from experiments and from the particle tracking with random walk diffusion method for (a) a rectangular channel, (b) staggered herringbone channel and (c) symmetric herringbone channel. The dimensions of the channels are listed in Table 1. The distance of measurement from injection is 22 cm. For all cases Pe ~ 10^4.

tal results and the particle tracking with random walk diffusion. For all the channels considered the agreement was good. As was shown in Section 4.1.1 for particle tracking, as the Pe number decreases, mass transfer by diffusion plays an important role and the impact of using herringbone structures to narrow the RTD is reduced. In Fig. 12, experimental RTDs for the three channel types are shown for a lower Pe $\sim 10^3$, obtained by decreasing liquid flowrate. The channels with herringbone structures still have a narrower RTD and lower variance (0.029, 0.033) than a rectangular channel (0.070), but the difference is not as great as in the case for Pe $\sim 10^4$ (compare with Fig. 10.).

5. Conclusions

Residence time distributions were obtained numerically via particle tracking with random walk diffusion and experimentally for a rectangular channel and the results were compared with a rectangular channel of the same dimensions with staggered and symmetric herringbone structures. Comparisons between RTDs obtained from simulations and experiments were in good agreement. Both simulations and experiments show that at high Peclet (Pe) numbers, channels with herringbone structures have a narrower RTD than a rectangular channel. However, this difference is reduced as Pe decreases. Simulations also showed that at high Pe the RTD for the herringbone channels remains unaffected. This result opens the possibility of increasing the dimensions of the channel without compromising its performance in terms of narrow RTD. The RTD for the channels with herringbone structures can be fitted to an axial dispersion exchanging mass with a stagnant zone model (ADEM). This was shown to be helpful to describe RTDs at long lengths. An analysis of the effect of the groove geometrical parameters on the variance of the RTD showed that a groove angle of $\theta = 45^\circ$, depth of $g_d = 31$ μm and width $g_w = 50$ μm is close to the optimum. By calculating the conversion for a first order chemical reaction, it was shown that the dimensions of the channel with herringbones can be significantly increased relative to a plain rectangular channel without affecting its performance.

Acknowledgments

ACP would like to thank the scholarship granted by the Mexican Council for Science and Technology (CONACyT-Mexico).

References

[1] A. Gavriilidis, P. Angeli, E. Cao, K.K. Yeong, Y.S.S. Wan, Technology and applications of microengineered reactors, Chemical Engineering Research & Design 80 (A1) (2002) 3–30.
[2] P.V. Danckwerts, Continuous flow systems—distribution of residence times, Chemical Engineering Science 2 (1) (1953) 1–13.
[3] G. Taylor, Dispersion of soluble matter in solvent flowing slowly through a tube, Proceedings of the Royal Society of London Series A-Mathematical and Physical Sciences 219 (1137) (1953) 186–203.
[4] R. Aris, On the dispersion of a solute in a fluid flowing through a tube, Proceedings of the Royal Society of London Series A-Mathematical and Physical Sciences 235 (1200) (1956) 67–77.
[5] O. Levenspiel, W.K. Smith, Notes on the diffusion-type model for the longitudinal mixing of fluids in flow, Chemical Engineering Science 6 (4–5) (1957) 227–233.
[6] D. Dutta, A. Ramachandran, D.T. Leighton, Effect of channel geometry on solute dispersion in pressure-driven microfluidic systems, Microfluidics and Nanofluidics 2 (4) (2006) 275–290.
[7] O. Levenspiel, Chemical Reaction Engineering;, third ed., John Wiley and Sons, New York, 1999.
[8] A. Günther, S.A. Khan, M. Thalmann, F. Trachsel, K.F. Jensen, Transport and reaction in microscale segmented gas-liquid flow, Lab on a Chip 4 (4) (2004) 278–286.
[9] F. Trachsel, A. Günther, S. Khan, K.F. Jensen, Measurement of residence time distribution in microfluidic systems, Chemical Engineering Science 60 (21) (2005) 5729–5737.
[10] W. Salman, P. Angeli, A. Gavriilidis, Sample pulse broadening in Taylor flow microchannels for screening applications, Chemical Engineering & Technology 28 (4) (2005) 509–514.
[11] W. Salman, A. Gavriilidis, P. Angeli, Axial mass transfer in Taylor flow through circular microchannels, AIChE Journal 53 (6) (2007) 1413–1428.
[12] J.T. Adeosun, A. Lawal, Mass transfer enhancement in microchannel reactors by reorientation of fluid interfaces and stretching, Sensors and Actuators B-Chemical 110 (1) (2005) 101–111.
[13] D. Boškovic, S. Loebbecke, Modelling of the residence time distribution in micromixers, Chemical Engineering Journal 135 (2008) S138–S146.
[14] A.D. Stroock, S.K. Dertinger, A. Ajdari, I. Mezic, H.A. Stone, G.M. Whitesides, Chaotic mixer for microchannels, Science 295 (5555) (2002) 647–651.
[15] J. Aubin, D.F. Fletcher, J. Bertrand, C. Xuereb, Characterization of the mixing quality in micromixers, Chemical Engineering & Technology 26 (12) (2003) 1262–1270.
[16] H. Wang, P. Iovenitti, E. Harvey, S. Masood, Numerical investigation of mixing in microchannels with patterned grooves, Journal of Micromechanics and Microengineering 13 (2006) 801–808.
[17] Y.Z. Liu, B.J. Kim, H.J. Sung, Two-fluid mixing in a microchannel, International Journal of Heat and Fluid Flow 25 (6) (2004) 986–995.
[18] T.G. Kang, T.H. Kwon, Colored particle tracking method for mixing analysis of chaotic micromixers, Journal of Micromechanics and Microengineering 14 (7) (2004) 891–899.
[19] J.T. Yang, K.J. Huang, Y.C. Lin, Geometric effects on fluid mixing in passive grooved micromixers, Lab on a Chip 5 (2005) 1140–1147.
[20] J. Aubin, D.F. Fletcher, C. Xuereb, Design of micromixers using CFD modelling, Chemical Engineering Science 60 (8–9) (2005) 2503–2516.
[21] C.A. Li, T.N. Chen, Simulation and optimization of chaotic micromixer using lattice Boltzmann method, Sensors and Actuators B-Chemical 106 (2) (2005) 871–877.
[22] M. Camesasca, M. Kaufman, I. Manas-Zloczower, Staggered passive micromixers with fractal surface patterning, Journal of Micromechanics and Microengineering 16 (11) (2006) 2298–2311.
[23] D.G. Hassell, W.B. Zimmerman, Investigation of the convective motion through a staggered herringbone micromixer at low Reynolds number flow, Chemical Engineering Science 61 (2006) 2977–2985.
[24] M.A. Ansari, K.Y. Kim, Shape optimization of a micromixer with staggered herringbone groove, Chemical Engineering Science 62 (23) (2007) 6687–6695.
[25] M.S. Williams, K.J. Longmuir, P. Yager, A practical guide to the staggered herringbone mixer, Lab on a Chip 8 (7) (2008) 1121–1129.
[26] S.P. Kee, A. Gavriilidis, Design and characterisation of the staggered herringbone mixer, Chemical Engineering Journal 142 (1) (2008) 109–121.
[27] A.D. Stroock, G.J. McGraw, Investigation of the staggered herringbone mixer with a simple analytical model, Philosophical Transactions A: Mathematical, Physical and Engineering Sciences 2004 (362) (1818) 971–986.
[28] M. Günther, S. Schneider, J. Wagner, R. Gorges, T. Henkel, M. Kielpinski, J. Albert, R. Bierbaum, J.M. Kohler, Characterisation of residence time and residence time distribution in chip reactors with modular arrangements by integrated optical detection, Chemical Engineering Journal 101 (1–3) (2004) 373–378.
[29] S. Lohse, B.T. Kohnen, D. Janasek, P.S. Dittrich, J. Franzke, D.W. Agar, A Novel method for determining residence time distribution in intricately structured microreactors, Lab on a Chip 8 (3) (2008) 431–438.
[30] O. Levenspiel, J.C.R. Turner, Interpretation of residence-time experiments, Chemical Engineering Science 25 (10) (1970) 1605–1609.
[31] J.D. Kirtland, G.J. McGraw, A.D. Stroock, Mass transfer to reactive boundaries from steady three-dimensional flows in microchannels, Physics of Fluids 18 (7) (2006).
[32] S.C. James, C.V. Chrysikopoulos, An efficient particle tracking equation with specified spatial step for the solution of the diffusion equation, Chemical Engineering Science 56 (23) (2001) 6535–6543.
[33] C.W. Gardiner, Handbook of Stochastic Methods for Physics. Chemistry and the Natural Sciences, Springer Verlag, Berlin, 1983.
[34] C.Y. Wen, L.T. Fan, Models for Flow Systems and Chemical Reactors, first ed., Marcel Dekker, 1975.
[35] V. Ananthakrishnan, W.N. Gill, A.J. Barduhn, Laminar dispersion in capillaries. I. Mathematical analysis, AIChE Journal 11 (6) (1965) 1063–1072.
[36] C. Castelain, D. Berger, P. Legentilhomme, A. Mokrani, H. Peerhossaini, Experimental and numerical characterisation of mixing in a steady spatially chaotic flow by means of residence time distribution measurements, International Journal of Heat and Mass Transfer 43 (19) (2000) 3687–3700.
[37] C. Castelain, A. Mokrani, P. Legentilhomme, H. Peerhossaini, Residence time distribution in twisted pipe flows: helically coiled system and chaotic system, Experiments in Fluids 22 (5) (1997) 359–368.
[38] W.P.M. Van Swaaij, J.C. Charpentier, J. Villermaux, Residence time distribution in the liquid phase of trickle flow in packed columns, Chemical Engineering Science 24 (7) (1969) 1083–1095.
[39] M.T. Kreutzer, J.J.W. Bakker, F. Kapteijn, J.A. Moulijn, P.J.T. Verheijen, Scaling-up multiphase monolith reactors: linking residence time distribution and feed maldistribution, Industrial & Engineering Chemistry Research 44 (14) (2005) 4898–4913.
[40] M.A. Fahim, N. Wakao, Parameter-estimation from tracer response measurements, Chemical Engineering Journal and the Biochemical Engineering Journal 25 (1) (1982) 1–8.
[41] M.L. Michelsen, K. Ostergaard, Use of residence time distribution data for estimation of parameters in axial dispersion model, Chemical Engineering Science 25 (4) (1970) 583–592.

[42] N. Wakao, S. Kaguei, Heat and Mass Transfer in Packed Beds, Gordon and Breach, Science Publishers Inc., New York, 1982.
[43] O. Levenspiel, B.W. Lai, C.Y. Chatlynne, Tracer curves and residence time distribution, Chemical Engineering Science 25 (10) (1970) 1611–1613.
[44] E.B. Nauman, B.A. Buffham, Mixing in Continuous Flow Systems, John Wiley & Sons Inc., New York, 1983.
[45] T. Liliedahl, K. Sjostrom, L.P. Wiktorsson, Analysis Method of Pyrolysis Kinetics Using Modern Signal-Processing Techniques, AIChE Journal 37 (9) (1991) 1415–1419.
[46] P.L. Mills, M.P. Dudukovic, Convolution and deconvolution of nonideal tracer response data with application to 3-phase packed-beds, Computers & Chemical Engineering 13 (8) (1989) 881–898.
[47] H.S. Song, S.P. Han, A general correlation for pressure drop in a kenics static mixer, Chemical Engineering Science 60 (21) (2005) 5696–5704.
[48] A. Vikhansky, Effect of diffusion on residence time distribution in chaotic channel flow, Chemical Engineering Science 63 (7) (2008) 1866–1870.
[49] N.S. Lynn, D.S. Dandy, Geometrical optimization of helical flow in grooved micromixers, Lab on a Chip 7 (5) (2007) 580–587.